https://doi.org/10.5194/egusphere-2025-4669
Preprint. Discussion started: 7 October 2025

Image-based tracking of mixed-sized surface sands and gravels under ultraviolet lights in a shallow flume

Megan Iun[1,2], F. Asal Montakhab[1,3], Lukas Mueller[1,4], Bruce MacVicar[1]

[1]Department of Civil and Environmental Engineering, University of Waterloo, Waterloo, N2L 3G1, Canada
[2]GHD, Waterloo, N2L 3X2, Canada
[3]Geoprocess Research Associates, Dundas, L9H 6Y6, Canada
[4]GEI Consultants Canada Ltd, Kitchener, N2E 3J2, Canada

Correspondence to: B.J. MacVicar (bmacvicar@uwaterloo.ca)

Abstract. Simultaneous characterization of the size and organization of both static and moving sediment particles would help to better understand bedform development in river channels. In the current study, an image-based particle tracking method was developed to measure the pathways of sediment particles in transport and visualize their interactions with evolving sedimentary bedforms in flume experiments. The method is novel because it: i) uses ultraviolet lights, fluorescent paint and image segmentation to obtain size class-specific videos of sediment transport over a mixed bed; ii) applies a blob-detection method included in a standalone software (TracTrac – Heyman, 2019) to detect and track particles at rest and in motion; and iii) includes a custom post-processing algorithm that includes a grid-based probabilistic motion model to minimize error in the inferred connections between particle positions on a path. We applied the algorithms on a set of videos taken during a laboratory experiment in which a pair of alternate bars and a cross-over central bar were forming in a shallow flume with non-cohesive sand and gravel transport. When the method works well, as it did for the case of particles in the 2.4-4.0 mm size class (~7 pixels in nominal diameter), the method resulted in an error of +7% for the number of tracks and -20% for the average duration of tracks. This degree of accuracy allowed us to analyse the locations of static particles and sediment pathways to show how the active sediment corridor shifted across the frame and then changed angles from the initial trajectories as the set of bars developed. Success of the method is reliant on accurate detection of tracer positions and the ability to predict connections between two identified positions with a motion model. Recommendations are given for application of the method and further testing to reduce reliance on subjective parameters.

1 Introduction

The movement of sediment in fluvial and aeolian environments is fundamental to understanding how landscapes are formed and how human actions may alter these environments, yet the direct measurement of sediment in motion remains a vexing technical challenge. The physical reality of the process is complex, with the rate and size distribution of transported sediment dependent on the interactions between the grains in transport, the shape and roughness of the surface of the sediment, and the fluid stresses applied in a turbulent environment with complex feedbacks operating at different temporal and physical scales.

https://doi.org/10.5194/egusphere-2025-4669
Preprint. Discussion started: 7 October 2025

For particles transported as bedload, which are in contact at least intermittently with the solid surface, the interaction between the surface texture and bed load transport is critical (Wilcock, 2001), meaning that prediction of sediment output, normally written as a function of excess fluid shear stress, also requires knowledge of the size and organization of particles on the surface of the sediment bed (Wilcock and Crowe, 2003; Ferrer-Boix and Hassan, 2014). With this need to know the state of the system in order to predict the response, the difficulty of obtaining reliable measurements is a knowledge-limiting problem (Ancey, 2020a). It seems to be difficult or impossible to remove 'noise' from transport data – meaning that spatial variability and temporal fluctuations are intrinsic features of bedload transport (Ancey, 2020b). Measurement methods that are able to describe the state of the bed and capture the spatial and temporal kinematics of sediment transport are likely to lead to new insights.

The link between the state of the surface of the sediment cover and the sediment transport rate was firmly established with a series of experiment by Wilcock and McArdell (1993; 1997), who used an 'unusual' sediment bed in which each size fraction was painted a different color - the Bed of Many Colors (BOMC). With this innovative technique, they could reliably describe the size distribution of the sediment particles on the surface of the bed with photographs, from which they derived transport models for mixed size sediment (Wilcock and Kenworthy, 2002; Wilcock and Crowe, 2003). The BOMC approach has since been used by others using anywhere from five to 16 colors to investigate a range of questions related to sediment sorting and dispersion (Wong et al., 2007; Sklar et al., 2009; Ferrer-Boix and Hassan, 2014; Johnson et al., 2015; Chartrand et al., 2018; Reiterer et al., 2024). Many simpler (one or two color) painting schemes have also been used to answer questions related to particular fractions of the sediment load (Humphries et al., 2012; Battisacco et al., 2016; Mckie et al., 2021). Some experiments have also measured surface size distributions without color augmentation based on manual techniques (Mackenzie and Eaton, 2017), image-based sediment sieving techniques (Nelson et al., 2010; Nelson et al., 2014; Bankert and Nelson, 2018), and/more generalized image analysis packages such as ImageJ (Hodge et al., 2016). Although these techniques can provide accurate snapshots of the bed state at specific moments, they typically require the experiment to be stopped or paused for data acquisition, which can change the morphology, and do not attempt to track the paths of discrete particles over the bed.

Sediment tracers have been widely used in field studies (Hassan and Roy, 2016; Liébault et al., 2024). Methods have included image-based tracking of particle displacements by Drake et al., (1988) and others (Paiement-Paradis et al., 2011) to understand the relation between coherent turbulent events and transport. However, the video analysis procedures used manual techniques that limited the respective analyses. Such techniques are much easir to apply in the lab, and image-based tracking has been widely used to understand the interaction between sediment bedforms and particles in motion. Iseya and Ikeda (1987), for example, used fluorescent tracers in a straight flume and observed that the average velocity of gravel was higher than that of the sand in a mixture of the two, informing underlying mechanisms behind pulsations in transport rate despite constant forcing conditions. Lisle et al. (1991) also visually tracked gravel and sand tracers to describe the impact of coarse sediment deposition in shallow areas on lateral flow deflection and the formation of non-migrating alternate bars. Pyrce and Ashmore (2003, 2005) used fluorescent tracers to understand sediment pathways in a sinuous pool–bar morphology – adding tracers by hand, noting their pathways, and recording deposition locations in the dry. Key datasets of particle activity and velocity distributions have

https://doi.org/10.5194/egusphere-2025-4669
Preprint. Discussion started: 7 October 2025

been extracted from high resolution video (Roseberry et al., 2012; Fathel et al., 2015), but these latter works concluded with a call for the development of automated particle tracking methods.

Automatic methods have been developed for image-based tracking in a flume. In most cases, researchers have augmented the contrast of tracers relative to the background to better isolate the particles. For example, a method developed by Zimmerman et al. (2008) and applied by others (Elgueta-Astaburuaga and Hassan, 2017; Elgueta-Astaburuaga et al., 2018) routes the sediment output over a light table so that sediment size can be measured and the transport rate calculated. Lajeunesse et al. (2010) worked in a relatively small flume with images taken through the water surface for an experiment in which 10% of the sediment particles were dyed black so that they could be reliably detected and tracked using an unnamed algorithm. Fan et al. (2017) also used a simple flume apparatus, with 50 tracers released over a fixed bed to facilitate tracking of their displacements using the ImageJ software package. A particle tracking software called Streams has been developed (Nokes, 2012), which is a fairly broad set of tools for flow visualization that includes particle tracking velocimetry (PTV). The software can be used to extracts the movement of discrete particles using a differencing technique (Radice et al., 2017; Campagnol et al., 2015; Ermilov et al., 2022; Rebai et al., 2024). In most applications, a highly simplified flume setup has been used, primarily using white tracers over a dark background to maximize the contrast. Similar methods have been developed by Terwisscha van Scheltinga et al. (2021), who used the natural coloration of the mix of volcanic and sedimentary sediment to achieve the necessary contrast. Heays et al, (2014) used a BOMC approach with six classes to extract particle paths using image differencing in a relatively complex environment with a mixed size bedload. The Heays algorithm is particularly advantageous because it can characterize both the state of the bed surface and the particle tracks, which led to a better understanding of how the particles were moving through the microtopography of the bed. However, the technique has not been widely applied and remains dependant on image differencing for tracking. An alternative approach to movement detection could use blob detection algorithms of the type used in the software TracTrac (Heyman, 2019). Such algorithms were shown to be more efficient for tracking objects at high densities and image frame rates, but the motion model applied does not distinguish between static particles and those in motion and does not consider time gaps for missing detections. Given the inherent noisiness of sediment transport and the problem of particles existing both at rest and in motion on the bed, there is a need for motion models specific to sediment transport.

The goal of the current study was to advance a technique using fluorescent tracers to track the motion of particles in mixed fluvial bedload transport. The experiments followed earlier work by Peirce et al. (2021) to model the effect of sediment feed rate and size distribution on bedform development, and earlier experiments with fluorescent tracers by Pyrce and Ashmore (2005). Specific objectives of the study were to: a) develop and validate a method that would apply and utilize blob detection algorithms to detect and track static and mobile sediment particles; and b) apply the method to document the evolution of sediment transport pathways and bedform development during a period of alternate bar growth in a flume experiment. Given the need to visualize sedimentary bedform development in a shallow flow and conditions of partial transport, it was necessary to place the camera above the water surface, develop methods to address the intermittency of particle detection, and distinguish between static and moving particles in motion models. Computer codes and samples are provided for other researchers to use as a basis for their own investigations (github.com/macvicab/ParticleTracker/).

https://doi.org/10.5194/egusphere-2025-4669
Preprint. Discussion started: 7 October 2025

2. Methods

2.1 Flume

Physical experiments were performed in a 13.3-m long, 2-m wide tiltable flume located at the University of Waterloo (Figure 1). The physical scale model used for these experiments was based on a section of Wilket Creek in Toronto previously researched as part of a restoration project (Papangelakis and Macvicar, 2020) and has used to assess the feasibility of sediment augmentation for bedform reconstruction (Peirce et al., 2021). Field surveys of the irregularly meandering thalweg and variable channel width were used to construct a 1:40 scale model of the reach. The experimental water discharge (Q_m) of 1.93 Ls^{-1} was established based on Froude-scaling following Frostick et al., (2011) and a field scale discharge of Q = 19.5 m^3s^{-1} based on a 2-year return period discharge estimate from a hydrologic study (AECOM, 2011). Discharge was steady through the experiment and controlled using a V-notch weir at the outlet of the head tank and monitored with a hook gauge. The flume slope was set to 1.5%, approximating the valley slope of the field reach and translating to an average bed channel slope (S_o) of 1.1%.

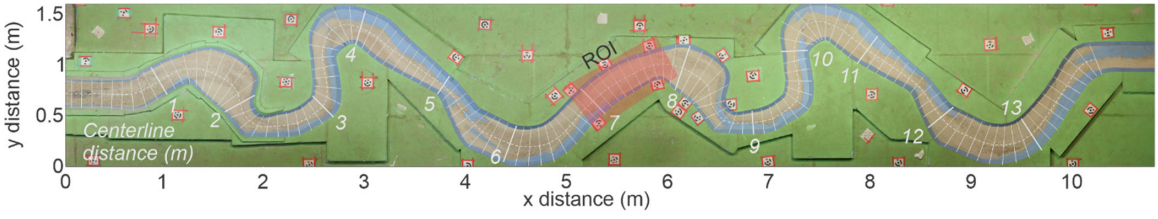

Figure 1 – Orthomosaic image of flume showing the region of interest (ROI) for the video recording. Centerline distances are spaced at 0.10 m intervals. The underlying image shows the bed after the experiment at an equilibrium condition where the feed rate is equal to the rate of sediment export from the channel.

The experiment was started from a bare bed condition to simulate the underlying clay till parent material of the regional geology (Bevan et al., 2018). Sand grains (0.7–1 mm) were glued sparsely over the bed and banks of the channel and covered with a blue epoxy paint to match the relatively smooth clay substrate with occasional coarse particles that was observed at the field site, some of which is still visible in the uncovered areas of the orthomosaic example image (Figure 1). A constant sediment feed rate (Q_s) of 4 gs^{-1} was used to allow comparison with an experiment described by Peirce et al. (2021), who estimated the sediment capacity of the channel (Q_c) to be 8 gs^{-1}. The feed mixture had a D_{50} of 0.92 mm and a D_{84} of 2.3 mm (Figure 2a). Starting from a bare bed condition, this feed rate resulted in a ~60% cover of the bed with alluvial sediment after 4 hours and an equilibrium bed cover of ~69% after 6 hours.

A trolley consisting of a steel frame mounted on rails beside the flume was used to position cameras and lighting equipment at heights up to 2.5 m above the bed of the flume. To allow in-flood video tracking of sediment in motion, a fraction of the particles was painted with fluorescent colors so that they shone brightly under ultraviolet lights (Figure 2). Based on a preliminary assessment of color segmentation, a three-color BOMC approach was adopted, with tracers in the largest size fraction painted pink (4 to 5.6 mm), a second painted green (2.36 to 4 mm), and a third painted orange (1.18 to 2.36 mm).

https://doi.org/10.5194/egusphere-2025-4669
Preprint. Discussion started: 7 October 2025

Particles that were less than 1.18 mm were not painted. Based on visual observations of the final mixture and the desire to not overwhelm the accuracy of the particle tracking software, it was decided to paint 25% of the 4 to 5.6 mm class, 12.5% of the 2.36 to 4 mm, and 5% of the 1.18 to 2.36 mm. With this distribution, the tracers could be easily seen under typical experimental conditions (Figure 2d).

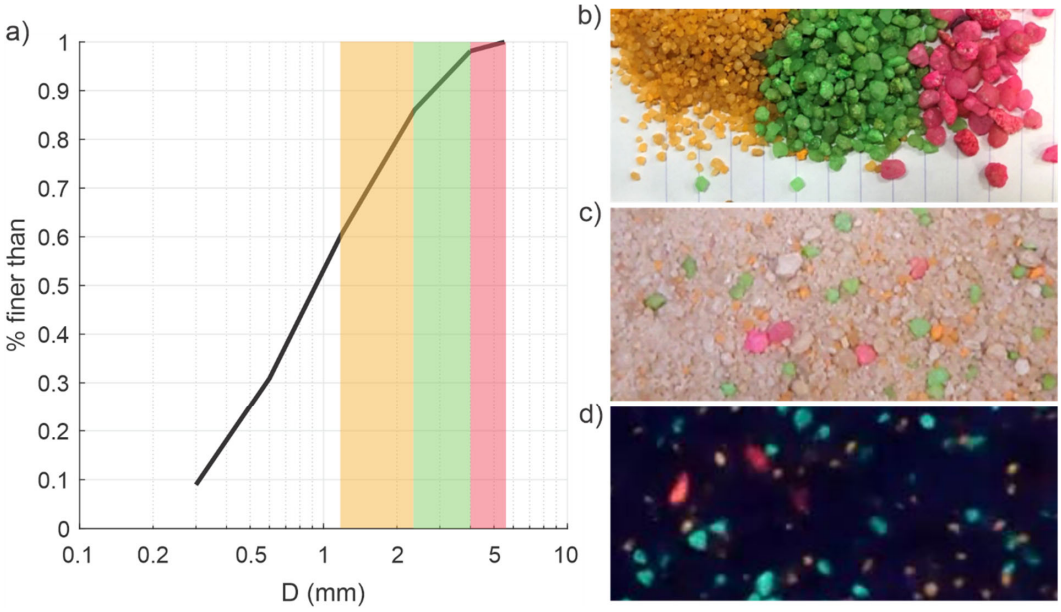

Figure 2 – Grain size distribution and tracers including a) grain size distribution with fractions with painted tracers indicated by color bands; b) three sizes of tracers after painting; c) tracers mixed with rest of sediment under fluorescent lights; and d) sediment illuminated under ultraviolet light during an experimental run.

2.2 Video Recording

A Panasonic-DC-BGH1 camera was used for the current experiment. Camera settings were set to record at 60 frames per second (fps) and a resolution of 1080 x 1920 pixels (px). The camera was connected to a computer via Ethernet cable and controlled using the Lumix Tether for Multicam application supported by Panasonic. During video recording, a black plastic sheet was used to cover the camera cage to prevent external light pollution, and the bed was illuminated with ultraviolet (UV) lights so that the painted particles were clearly visible (Figure 2d). Two LED 100 W equivalent UV lights were suspended from the camera cage at elevations approximately 1 m above the channel. Lights were angled to minimize reflectance on the water surface.

The camera was set to record within a region of interest (ROI) during the experiment. The ROI covers a straight section between two bends that is ~1.05 m long in the streamwise direction and covers the full width of ~0.25 m of the channel (Figure

https://doi.org/10.5194/egusphere-2025-4669
Preprint. Discussion started: 7 October 2025

1). The ROI is far from the upstream and downstream ends of the channel so that it is relatively unaffected by the boundary conditions. The water surface was relatively flat during the experiments, which meant that surface reflections were minimal. Four 10 s sections of the video (600 frames each) were selected from the video recordings to analyze a time period between 50 to 110 min since the beginning of the experiment. The time period was selected because alternate point bars and a cross-over riffle developed in the ROI during that time. The increasing complexity of the bar structure allowed us to assess the performance of the algorithm during periods of both single-layer motion, where the bed was mostly uncovered and static and moving tracer particles were largely occurring in different areas of the bed, and overtopping motion, where some tracer particles moved over previously deposited particles.

2.3 Video Segmentation

To allow tracking of particles by size class, a custom MATLAB algorithm was created to create separate masked video files based on colour segmentation. Colour profiles were generated using an interactive MATLAB tool called `ColorThresholder`, which allows a user to select sample areas within an image, assess and modify the quality of the masking in an interactive way, and export a function with the created colour profile. For reference, Matlab algorithm names will be written in `Courier` font. Based on our tests, the most effective option was to transform the RGB raw images into CIELAB ($L^*a^*b^*$) color space, where L^*, a^*, and b^* represent Lightness (0 – black, 100 – white), red/green value (large positive – red, large negative – green), and blue/yellow (large positive – yellow, large negative – green), respectively. To reduce visible errors caused by imperfect segmentation, the masked images were post-processed using the image analysis algorithms called `imclose` (to remove small gaps between masked areas), `imfill` (to fill in areas that are completely enclosed by masked areas), and `bwareafilt` (to filter out small, masked areas).

An example of a raw image and the image segmentation for the green particles is shown in Figure 2. The green particles have a range of brightness values in the raw image and range in size from just a few pixels in diameter to over 10 pixels. The intermediate stage of masking eliminates particles in other colours such as the small orange particles visible in Figure 2a. The final stage stretches the brightness of the masked image over the three colours so that the brightest green areas appear as white against the black background (Figure 2c). New colour profiles were generated for each experimental run due to slight variations in lighting and camera position. To assist with the video segmentation procedure, a Matlab code was written along with a simple guide.

https://doi.org/10.5194/egusphere-2025-4669
Preprint. Discussion started: 7 October 2025

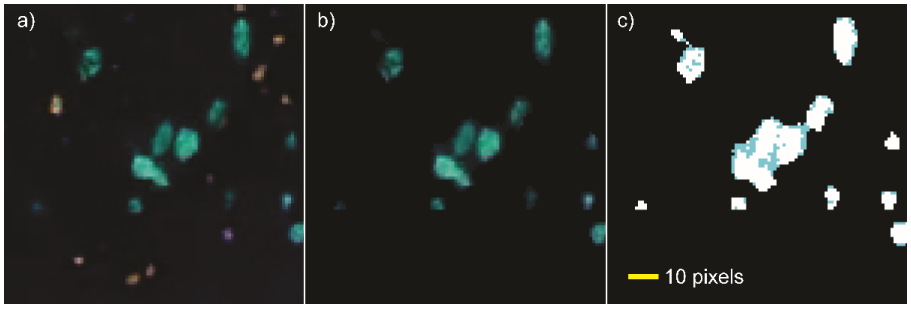

Figure 3 – Image segmentation including a) a sample raw video frame (100x100 pixels); b) masked raw image based on green segmentations (particles are 2.36 to 4 mm); and c) processed video frame used.

2.4 Particle tracking

Particle tracking was completed in two phases. In the first phase, the color-segmented video files were inputted to TracTrac (Heyman, 2019) to get a preliminary result. In the second phase, the preliminary results were analysed in a custom post-processing algorithm to improve the results. To help with the description of the tracking procedure, we will use the following definitions:

- Position – a detected particle object location (i, j) within an image frame (f);
- Tracklet – two consecutive positions of an identified particle $(i_1, j_1, f_1;\ i_2, j_2, f_2)$;
- Track Segment – a series of tracklets of an identified particle; and
- Track - the 'true' and complete set of locations $\{i, j, f\}$ that a particle takes.

The overall goal of the particle tracking procedure is to obtain a set of automatically detected track segments that match the particle tracks in a video recording. Tracks were established using a manual validation procedure as described in section 2.5.

The TracTrac algorithm is advantageous primarily because: 1) it uses a blob detection algorithm to detect objects, which we wanted to test for sediment particle tracking, 2) it includes a motion model to predict tracklets, 3) is open-source and therefore useful for understanding the impact of different steps in the analysis, and 4) it has many tunable parameters that can be adjusted for different applications. The algorithm was not developed for sediment transport tracking, however, and its novel application to the problem eventually required some post-processing. For the current analysis, a manual optimization of tunable parameters was completed. Parameter values that were found to perform the best for all videos in the current study are listed along with the rationale in Table 1. Further work on the tuning of the "blob scale" and "peak neighbors" parameters are presented as part of the results because of the sensitivity of these values to the particle size. Post-processing is described in section 2.5.

Table 1 Parameter values used for the TracTrac (Heyman, 2019) phase of particle tracking

Parameter class	Parameter name	Value	Rationale
Image Processing	Background Model	Off	Removing static areas of the image was not desirable because particles were both static and moving within the ROI.

https://doi.org/10.5194/egusphere-2025-4669
Preprint. Discussion started: 7 October 2025

Parameter class	Parameter name	Value	Rationale
	Noise Filtering	On	Images tended to have small objects that we interpreted as noise in the color segmentation procedure.
Object Detection	Type	Bright	Particles are light objects against a dark background.
	Detector	Difference of Gaussians (DoG)	The DoG algorithm tends to result in elliptical objects that match with particle shapes.
	Intensity Threshold	Auto	Manual thresholds tended to produce unsatisfactory results and require extensive fine tuning.
	Sub-pixel Method	None	Sub-pixel refinement of object location was not necessary given that the uncertainty of pixel locations was more than one pixel.
Motion Model	Type	Unsteady	Particle motions are highly unsteady.
	Frames	3	This value for the running time average of the motion model performed satisfactorily.
	Iterations	3	This value for the number of iterations of the prediction/association process performed satisfactorily.
	Filter outliers	No	Filtering outliers tended to remove 'true' tracklets.

2.5 Post-Processing

The application of the TracTrac algorithm tended to result in: a) track segments that were shorter than the tracks that could be visually identified in the videos, and b) many isolated positions that were not part of any track segment. Based on the rationale that the motion model used by TracTrac was not developed for sediment transport, a post-processing algorithm was created (Figure 4). The rationale and logical flow of the key algorithm steps are briefly described below:

1. Break low probability tracklets (`addBreaks`). It was observed that the TracTrac results were sometimes skewed by long tracklets that were clearly erroneous. To remove these connections from the statistical analysis, breakpoints were identified using a hard-coded threshold for the maximum displacement distance (set at 15 pixels for the current study - specified as part of the input parameters in `particletrackingparameters`).
2. Calculate Statistics and Classify (`calcTrans`). Statistics including displacement distance, velocity, and acceleration were calculated for tracklets, and the cumulative duration and displacement distance were calculated for track segments. Track segments were classified as 'short' or 'long' (long segments were at least 5 frames in duration for this study), and 'static' or 'moving' (moving segments had a radial cumulative displacement distance of at least 10, 14 and 26 pixels for orange, green and pink particles, respectively). This algorithm is reapplied after all subsequent steps as pairs of track segments are combined.
3. Connect static and long track segments (`connectStaticLong`). It was observed from the videos that particles could be static for many consecutive video frames or even the entirety of the video segment, yet the Tractrac results were often discontinuous so that multiple track segments were identified at the same location at different times. We

https://doi.org/10.5194/egusphere-2025-4669
Preprint. Discussion started: 7 October 2025

therefore identified pairs of static track segments that were within a maximum radial distance from each other and at non-overlapping frames in the video sequence and combined them into a single-track segment. A loop was set up to check for progressively shorter track segments that fit within gaps of longer tracks to avoid connecting static particles with other particles that might be moving through the space. Short duration track segments were not connected to longer track segments in this phase because it was not possible to assess a priori whether they were static or moving.

4. Calculate grid-based motion models based on a Mahalnobis (2018) distance (`calcMahal`). The Mahalnobis distance allowed us to perform a probabilistic analysis for a two-parameter model, which was necessary because the displacement directions and magnitudes were highly correlated in the sediment displacement data The motivation for the motion model is similar to the algorithm used by TracTrac, which uses prior tracklets for each track segment to predict the direction and magnitude of subsequent tracklets. However, the new algorithm was developed based on the following observations: 1) typical particle displacement directions and magnitudes varied widely across the video frame, but were relatively consistent for a given location and time (e.g. static particles tended to remain static in certain areas of the video frame, while the moving particles tended to follow a consistent active transport pathway through the frame); 2) particles could move short distances in directions away from the active transport pathway, but were only likely to move long distances in the direction of the main transport pathway; 3) moving particles could pass close to or even intersect static particle positions, so that the two states could co-exist in any given area of the video frame; and 4) there could be multiple frames where it is difficult to identify discrete particles due to intersecting tracks or where a particle 'disappeared' for one or more frames due to water refraction or faint coloring issues. Based on these observations, the algorithm was written to divide the image frame into a grid (200 x 200 pixels for the current study) and calculate motion models based on all the tracklets of moving particles within each grid square. Two-component gaussian mixture models are fit to the z-scores of the magnitudes and angles of the tracklets, which meant that the covariance between these two variables is included in the models. Motion models are calculated for different time gaps to account for particles that are not detected in one or more frames. All motion models and basic statistics (mean and standard deviation) of the moving particle motions are then saved.
5. Connect moving track segments (`findlikelyMoving.m`). In this algorithm, the start time of each track segment is found and all other track segments that ended with a specified time gap before that are identified. The probability that these track segments are the same track is then tested by finding the Mahalnobis distance between the positions at the two endpoints of the track segments. The Mahalnobis (2018) distance is not a cartesian or polar distance, but rather a measure of the distance between a sample point and a probability distribution. Pairs of track segments where the distance was less than a confidence threshold (α) were connected. Based on tests with the analyzed videos, a value of $\alpha = 0.96$ was used for this study. The algorithm was written to loop through all track segments and look for progressively larger time gaps (up to 6 frames for this study).
6. Connect static short track segments (`connectShort.m`). Following the moving track segment connections, there were still short segment and 'free' detections remaining in the database. For this reason, a final check was completed

https://doi.org/10.5194/egusphere-2025-4669
Preprint. Discussion started: 7 October 2025

to look for static particles with short durations. Where they were within a maximum radial distance from other static track segments and at non-overlapping frames in the video sequence, the track segments were combined.

The codes for the post processing analysis are available at ** Github. A user's guide that includes a procedure to extract particle size parameters and run the TracTrac analysis is available at that location.

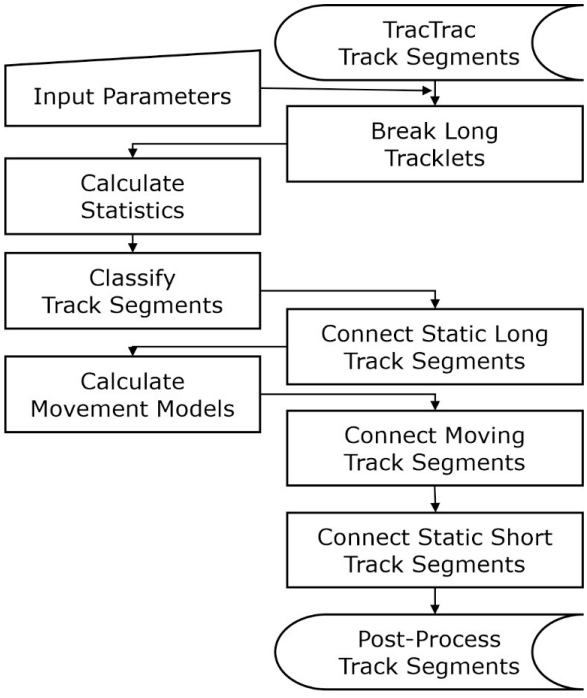

Figure 4 - Post-processing flow chart. Note that the step to calculate statistics and classify tracks is re-applied after each of the algorithms that connect track segments.

2.6 Validation

To develop a set of data for validation of the method, a graphical user interface (GUI) was created in Matlab. The GUI allows a user to select a Validation Region and then add annotations to indicate the positions of tracers in different images (Figure 5). The Validation Region can be saved and then loaded for other videos with the same viewpoint. To reduce the repetitive nature of the work, an option was added to allow the user to copy the tracer positions from the previous image. This option was used for the current application because most particles were stationary between two consecutive frames. The code was created for the current experiment, where three classes of sediment identified by color were analyzed, so the ability to separately annotate the orange, pink, and green tracers were provided. For the current study, all particle positions of all three tracer classes within a window 200 pixels wide (i = 800 to 1000) and 520 pixels high (j = 200 to 720) were annotated (Figure 5). The code for the GUI and manual annotations for one video are included in the Github repository.

https://doi.org/10.5194/egusphere-2025-4669
Preprint. Discussion started: 7 October 2025

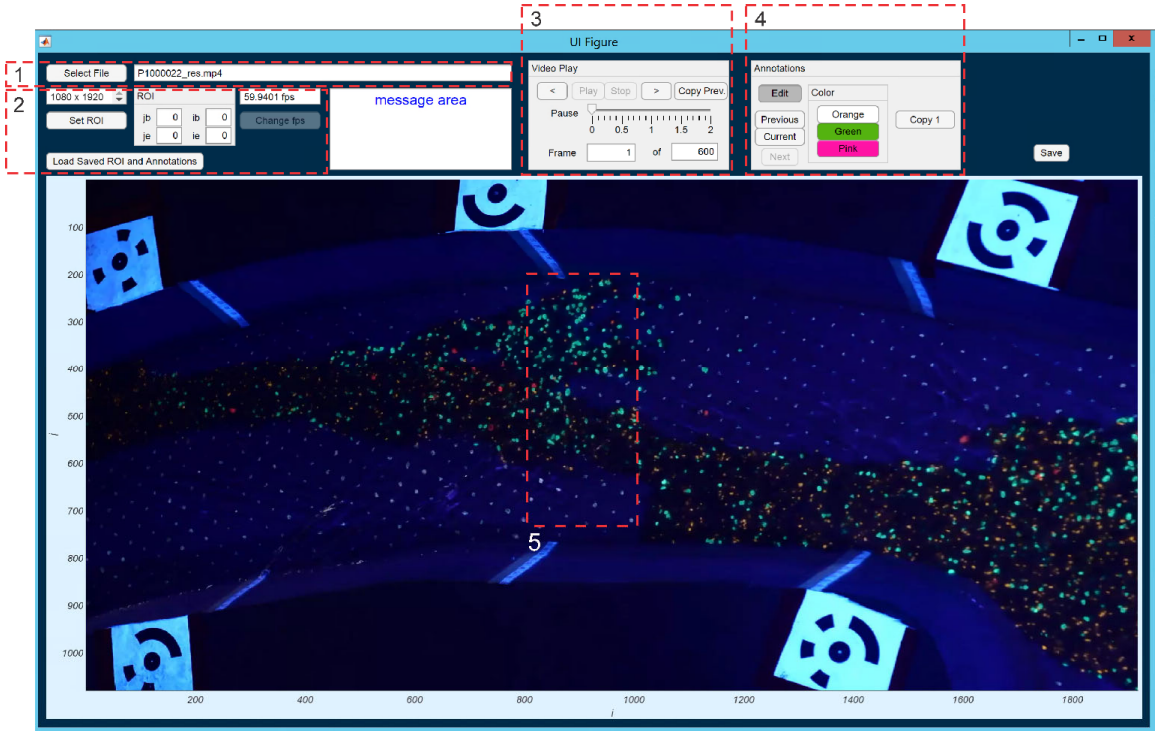

Figure 5 – Matlab GUI interface for manual tracking. Highlighted zones of the GUI include: 1) File information; 2) Region of Interest (ROI) information; 3) Video playback controls; 4) Annotations controls; and 5) Validation Region.

3. Results

3.1 Particle Tracking

Track segments that resulted from the application of the TracTrac algorithm were found to be highly sensitive to two parameters, the blob scale (C_{BS}) and the peak neighbors (C_{PN}). To better illustrate the issue and inform future applications of this approach, the effect of these parameters was tested. C_{BS} is a distance (px) that is used to scale a band-pass filter within a range of $\sqrt{2}C_{BS} \pm 20\%$ (Heyman, 2019). Objects smaller than the minimum of the band-pass filter range will tend to be blended with their surroundings, while objects larger than the maximum tend to be broken up into multiple objects. Using the green particles from Figure 3 as an example, a visual assessment of the masked raw image found that there are approximately 13 individual green particles that range in diameter from approximately 4 to 10 px, though results may vary between observers depending on how they understand the differences in brightness, shape, and inter-particle contact. A blob scale of 3 px filters the image into blobs that are 3.8 to 4.6 px in diameter and finds 17 possible particles, where some particles that appeared

https://doi.org/10.5194/egusphere-2025-4669
Preprint. Discussion started: 7 October 2025

spherical or oval in the original image now transformed into donut shapes with two possible object peaks (Figure 6). Increasing the blob scale to 5 or 6 px reduces this donut effect and finds the approximately correct number of particles, though the question of which ones are true particles and whether there are false or missing detections remains open. To understand the C_{PN} parameter, which is also a distance (px), it is important to know that the object locations are determined with the TracTrac algorithm by local maxima in image intensity after the filtering is applied (Heyman, 2019). To eliminate secondary peaks that are likely the same particle, C_{PN} sets the distance of a radial buffer surrounding the highest peak such that secondary peaks will not be considered discrete objects. The number of identified blobs in the frame decreases from 16 to 12 as C_{PN} is increased from 1 to 4 (Figure 7). For any application, it will be important for the user to determine appropriate values for these key parameters.

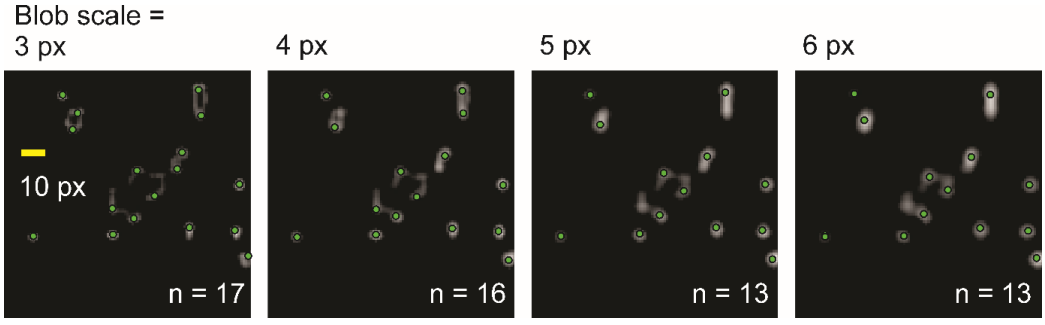

Figure 6 – Effect of the blob scale parameter (C_{BS}) on the filtered result of the processed video frameon object identification. The image region is the same 100x100 px region shown in Figure 3. A total of 13 green particles were identified in the region based on manual annotation. Peak neighbors (C_{PN}) = 3 px for these calculations.

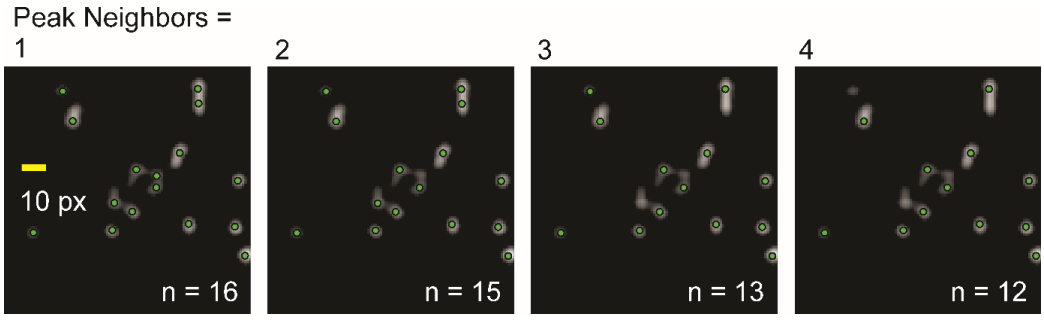

Figure 7 – Effect of the peak neighbours parameter (C_{PN}) on object identification. Image corresponds with 100x100 px region shown in Figure 3. A total of 13 green particles were identified in the region based on manual annotation. Blob scale (C_{BS}) = 5 px in these images so that image 3 corresponds with image 3 in Figure 6.

Particle size class metrics are summarized in Table 2, including information about the real-world sizes of the three sediment size classes used in the current study along with image parameters and implemented TracTrac parameters. Tracers represented 0.5-1.3% of the mass of sediment in the three tested size classes, with a smaller percentage of tracers added to smaller sizes

https://doi.org/10.5194/egusphere-2025-4669
Preprint. Discussion started: 7 October 2025

because they were more numerous. The relatively low percentage of tracers used was based on earlier experiments where it was found that the use of more tracers created more confusion for the tracking algorithm. To compare image measurements with the physical properties of the sediment, the image sizes of all non-touching particles were measured within the Validation Region for an image taken at a time from the start of the experiment (t) of 110 min. To avoid confusion where multiple particles were touching, only particles that appeared to be isolated from their neighbors were measured. Pink particles from slightly outside of the Validation Region were also measured to increase the number of pink particles included in the analysis. The length of the longest visible axis (L_a) and the perpendicular axis (L_b) were measured for a total of 57, 78 and 11 of the orange, green, and pink particles, respectively. The nominal diameter (D_N), which represents the diameter of a circle that has the same area as the assumed elliptical shape of the measured particle, and the sphericity (D_N/L_a) were calculated. A sphericity close to 1, which is typical of the particles in the image, indicates that the gaussian filter approach is likely to match the approximate shape of the particle and improve detection. For the two larger classes, the ratio of D_N to the mean of the size range ($\overline{D}$) was consistent (2.2 px/mm), but the smallest size class appeared larger (3.2 px/mm). It was noted during the measurements that the colour of the orange particles was often closer to white or blue, perhaps due to the blending of the particle color with the background around the edges of the particle, which also would made them appear relatively larger. Due to the small size of the orange particle, there remained only small areas that were identifiably orange in the recorded images. The TracTrac parameters were adjusted through subjective iterative testing, which means that an objective relation between image diameters and the parameters was not applied. Despite these ad hoc adjustments, the selected parameter values selected appear to follow a consistent pattern, with $D_N > C_{PN} > C_{BS} > C_{NF}$, and the ratios of the parameter values to $\overline{D}$ fall within relatively restricted ranges, other than C_{BS} for the orange particles, where the low value likely reflects the difficulty we had in finding suitable values for this size class.

Table 2 - Comparison of sediment size class, image measurements and applied TracTrac parameters for the three tracer classes used in the current study. The particle size classes are also represented as a percentile range from the cumulative distribution (p_D), the percentage of particles within the size class that were painted as tracers (p_C) and the mass of tracers within the size class relative to the total mass of sediment supply (p_m). For the image measurements, the average nominal diameter (D_N) and sphericity (Ψ) values are shown with the standard deviations included in parentheses. Measurements and TracTrac parameters are also shown relative to the mean sediment size ($\overline{D}$) for comparison.

Color	Sediment parameters				Image measurements			TracTrac parameters					
	D (mm)	p_D (%)	p_c (%)	p_m (%)	D_N (px)	$D_N/\overline{D}$ (px/mm)	Ψ	C_{NF} (px)	$C_{NF}/\overline{D}$ (px/mm)	C_{BS} (px)	$C_{BS}/\overline{D}$ (px/mm)	C_{PN} (px)	$C_{PN}/\overline{D}$ (px/mm)
Orange	1.2-2.4	61-87	5	1.3	5.0 (0.94)	3.2	0.87 (0.07)	1	0.55	1	0.55	3	1.7
Green	2.4-4.0	87-97	12.5	1.3	7.0 (1.3)	2.2	0.88 (0.08)	2	0.63	5	1.6	7	2.2
Pink	4.0-5.6	97-99	25	0.5	10.5 (1.7)	2.2	0.90 (0.06)	4	0.83	8	1.7	9	1.9

https://doi.org/10.5194/egusphere-2025-4669
Preprint. Discussion started: 7 October 2025

To help contextualise the experimental results, the frequency of detections within the Validation Region for the four analyzed videos were extracted from the manual results (Table 3). Tracer density increased in this area over time as more of the bed became covered with sediment. The mass of particles in each size class was estimated by dividing by the percentage of painted tracers and multiplying by a unit mass, assuming that all particles were spherical and had a diameter equal to the median of the range. The relative mass was then calculated by comparing this estimated mass for each size class with what is expected from the CDF of particle sizes by weight (Figure 2a). With this metric, size classes that are overrepresented on the bed surface have a relative frequency > 1 and vice versa. As shown, green particles are overrepresented in all videos, while the other sizes are underrepresented. All relative frequencies are trending towards 1.0 as the time increases, which is the expected distribution in an equilibrium condition. These results match what was expected from a replicate of the experiment in earlier work (Peirce et al., 2021), where particles > 2.8 mm were initially overrepresented in sediment exported from the flume while smaller size fractions were initially underrepresented but trended towards equilibrium over time.

Table 3 – Count and relative frequency of tracers in the videos analyzed in this study. The relative frequency is a ratio of the count to the number of tracers expected for each size fraction based on the size distribution of the sediment feed (shown in Figure **)

Video Name	t (min)	Orange		Green		Pink	
		Count	Relative Frequency	Count	Relative Frequency	Count	Relative Frequency
P000020	50	22	0.20	80	3.21	2	0.34
P000021	70	62	0.35	116	2.84	3	0.31
P000022	90	150	0.52	154	2.35	7	0.45
P000023	110	214	0.61	168	2.11	10	0.53

The manual detections of the green and orange particles are compared with the TracTrac-derived track segments to better understand the limitations of the algorithm (Figure 8). The correspondence between manual and automated analysis appears to be reasonable where tracer numbers are low (for example for the video at $t = 50$ min). For green particles in this video, there are few green dots (representing the automatic detections) that are not covered by black dots (representing the manual detections), and the automatic and manually derived paths seem more or less the same. To verify, the cases where particles were detected automatically but not manually were reviewed. It was confirmed that a manual error can occur when particles are confused with the dots on the bed of the flume (which were used to visualize where the bed was covered by sediment). The corresponding error (i.e. where dots might be confused with actual particles) was not made by the automatic algorithm, indicating that the color segmentation of the green particles was quite accurate. Occasional errors also occurred at the edges of the Validation Region, where particles were not always marked manually because their centre of mass appeared to be outside the Validation Region. More common errors occurred where the particles were in motion and not visible in all frames. In the automated code, new track segments are created for particles that are not detected for one frame or more, which means that a single track can be broken into track segments in the automated procedure. This type of error occurs in all cases, with the

https://doi.org/10.5194/egusphere-2025-4669
Preprint. Discussion started: 7 October 2025

exception of the green particles at $t = 50$ min, and is most obvious in the green particles at $t = 110$ min. Detection problems are common for the orange particles, and severe problems are evident with the path analysis. As shown for the $t = 50$ min video of the orange particles, for example, some tracks only had a couple of isolated positions detected and the positions are not connected in track segments. Static positions are reasonably well reproduced, but it is apparent that positions of particles cannot be accurately determined when they are small and moving quickly. This error is thought to be caused by the irregular water surface, which can result in particles appearing to 'vibrate' in place when they are not moving or 'flickering' as it travels through the region of interest, and the dimming of particles when they are moving quickly.

Though relatively rare, anomalous connections were also sometimes observed in the automatic analysis, for example, for the orange particles in the $t = 50$ min video at about $i = 840$ -890 px and $j = 400$ px, which is not close to any manually detected path and is long relative to typical displacement lengths. This type of error was thought to be related to the motion model, which uses past motions to make future predictions. For a new track, the motion model would have little information with which to predict the motion of a particle, so incorrect inferences are possible.

https://doi.org/10.5194/egusphere-2025-4669
Preprint. Discussion started: 7 October 2025

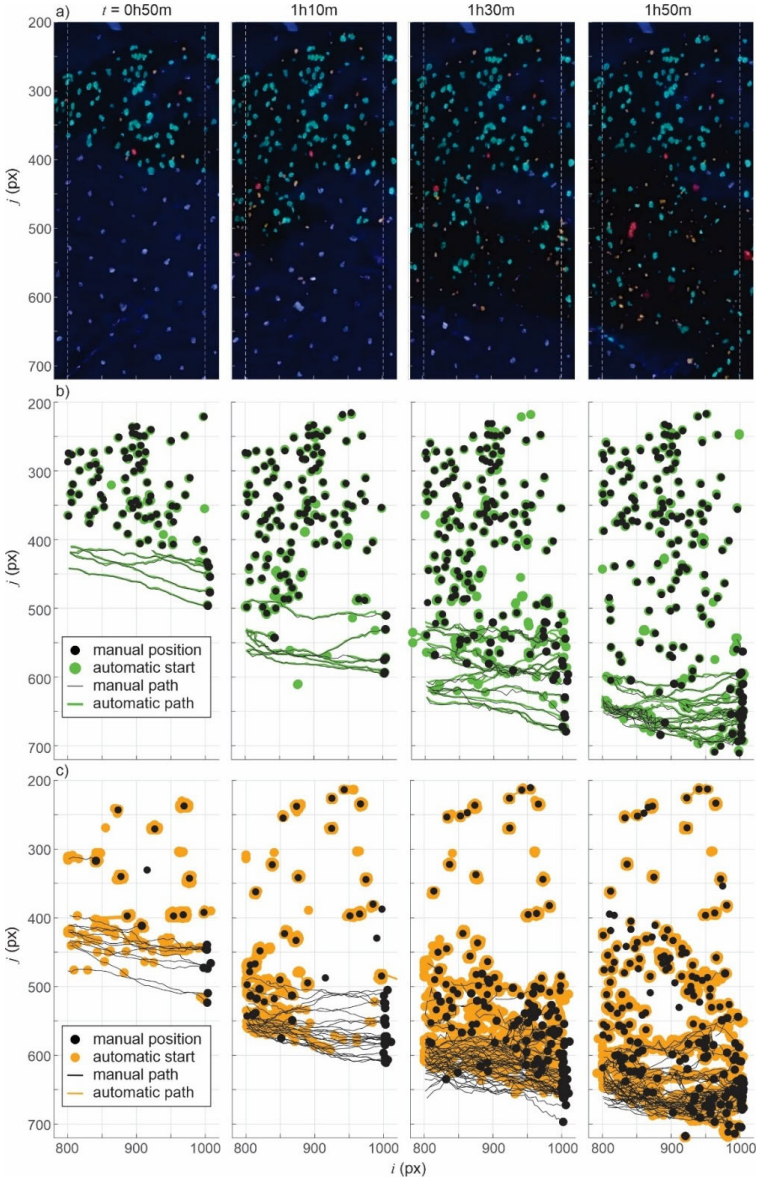

Figure 8 – Comparison of manual and automated tracking results for 10 s of particle motion within the Validation Region including: a) still images at the start at the start of each video, and results for b) green and c) orange particles. Results include manually annotated 'true' tracks, automatically detected track segments, and final positions of tracks and track segments. Each column shows the image still and results for 10 s video segments taken approximately 20 min apart (Table 3). For the track segments, the particle position is only shown for the final recorded position, making the automatically derived segments appear like beads on a string when they are discontinuous along the manually derived tracks.

https://doi.org/10.5194/egusphere-2025-4669
Preprint. Discussion started: 7 October 2025

3.2 Post-processing

To confirm the types of errors in the TracTrac segments and assess the impact of the post-processing steps, the number of particle detections per frame, the total number of track segments, and the average duration of the track segments were compared relative to the manually derived results (Figure 9). Error is introduced in the video segmentation and blob analysis stage, particularly for the smallest, orange particles, which identified an average >30% more particles than in the manual detection (Figure 9a). In contrast, the numbers of both the green and the pink particles were underestimated, with the green particles consistently under-detected by 15-20% and the pink particles showing a greater variability, with underestimation as high as 50%. The total number of track segments from the TracTrac analysis typically far exceeds the true tracks, which supports the idea that track segments are only capturing portions of the tracks (Figure 9b). Orange tracers are the clearest example, with the initial TracTrac result leading to > 1000% more track segments than tracks. Following post-processing, the number of tracks was reduced by orders of magnitude but still remain high in comparison with the manual results. If we consider only the long tracks, which essentially treats the isolated detections as errors, then the error in the number of track segments drops to ~70% for the orange particles and <10% for the green particles. Pink particles had similar improvements, though the fewer numbers of tracks identified by TracTrac and the low overall numbers of particles means that the significance of the results are not clear.

Track segments are reduced in number during the post processing because they are connected to other segments, which increases their overall duration (Figure 9c). This effect is most clearly seen for the green tracks, where the negative error on the time duration of the tracks indicates that they are relatively short compared to the manual results. After post-processing, the average duration of the green track segments is only ~20% less than the manual tracks, which shows that track segments are approaching the complete tracks. For the orange size class, for example, the duration increases from an almost -100% error to a mean of 30-40%, while the duration of the pink tracks becomes less variable due to post-processing, but the mean does not increase significantly and remains ~-40%. The high variability of the pink particle detection is again likely related to the relatively small numbers of particles in the Validation ROI (Table 3).

https://doi.org/10.5194/egusphere-2025-4669
Preprint. Discussion started: 7 October 2025

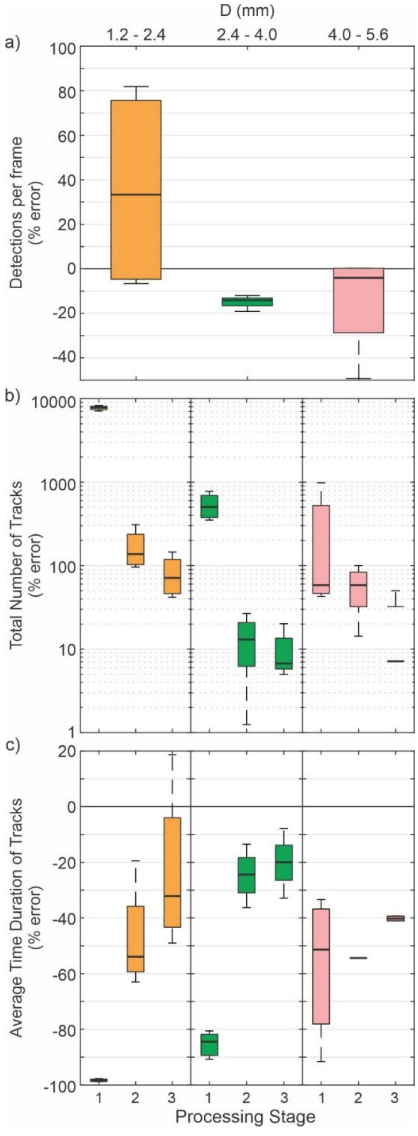

Figure 9 – Effect of postprocessing on detection statistics on particle detection and track segment metrics in comparison with manual annotation for three sizes of sediment particles. Processing stage refers to 1 – TracTrac output, 2 – all track segments after post-processing, 3 – only 'long' (> 5 frames) track segments after post-processing.

To visualize the paths of moving particles in relation to static particles, the tracks of the green particles were plotted over the full ROI for all four analyzed videos (Figure 11). For orientation, flow is from left to right and we refer to the 'far' and 'near' sides of the channel as the upper and lower parts of the image, respectively. Static and moving particles were differentiated for

https://doi.org/10.5194/egusphere-2025-4669
Preprint. Discussion started: 7 October 2025

this visualization, with the static particles represented by their mean position and the moving particles by the series of positions in the track segment. The result represented by Figure 11 demonstrates the utility of the method for the interpretation of deposition patterns and bar development as a function of the sediment transport pathways. For the video at $t = 50$ min, a delta shaped pattern of static particles is visible on the far side of the channel. The experiment began with a bare bed, so these particles represent the sediment deposited between $t = 0$ to 50 min and the collection of the tracers represents a sediment bar. This delta shape deposit is relatively symmetrical, but the transport around the bar is not, with all of the observed pathways occurring on the near, lower side of the bar. By $t = 70$ min, considerably more deposition has occurred, largely on the near side of the bar where transport is most active, but a few new static particles on the far side of the bar indicate that transport and bar growth can occur in that area. Nevertheless, the growth of the bar is asymmetric and the yellow static particles, which represent the deposited particles between $t = 50$ to 70 min, document the lateral growth of the bar towards the centre of the channel. At the same time, a new group of static particles is visible on the lower part of the image (centered at $i \approx 1300$ px and $j \approx 700$ px), which shows the growth of an alternate bar on the opposite side of the channel and below the dominant transport corridor for both the $t = 50$ and $t = 70$ min videos. In the later videos, we can see upstream progression of the lower bar, with particles deposited at $j \approx 700$ px and as far upstream as $i \approx 1050$ px and $i \approx 950$ px for the $t = 90$ and 110 min videos, respectively. In the $t = 90$ min video there is no visible gap in the positions of the static particles, which indicates that the alternate bars were connected by continuous sediment cover at this time. The effect of the continuous sediment cover means that there was no longer a continuous pathway over the bare bed so that the particles had to travel up and over the previously deposited particles. The effect of the cover on particle pathways is most visible for the $t = 110$ min video. In the upstream part of the frame, the particles largely travel on the near side of the bar in an area that had no static particles and no bed cover. When they reach the upstream limit of the bar on the near size of the image (at $j \approx 950$ px), the moving particles interact with the deposited particles and they change their direction to move away from the near side and around the bar that is developing.

https://doi.org/10.5194/egusphere-2025-4669
Preprint. Discussion started: 7 October 2025

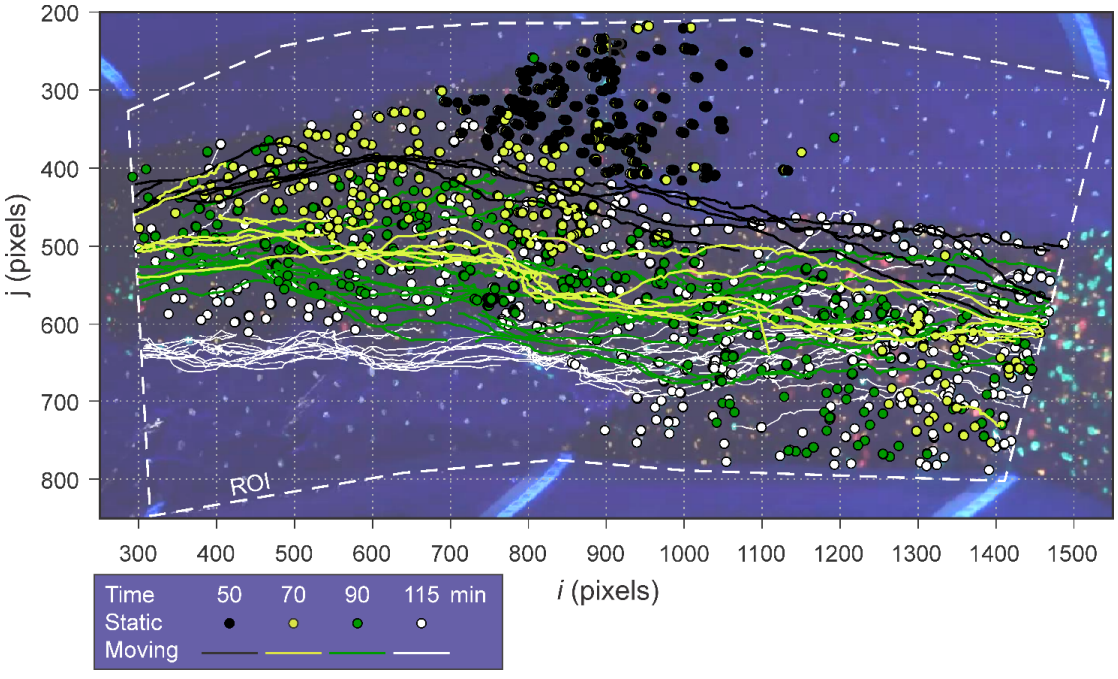

425

Figure 10 – spatial plot of paths and static green particles for 4 different videos, with the time indicating the time since the beginning of the experiment. The positions from the videos were plotted in reverse chronological order so that those from the first video are on top and detections from later videos at the same location are obscured. The Region of Interest (ROI) is indicated. The sides of the channel extend from the top and bottom edges of the ROI. Measurement tapes are visible at some locations where manual measurements of water level were made during the flume experiment. Flow direction is from left to right.

430

A key step of the post-processing method we developed uses a set of movement models to assess the probability of possible tracklet connections. These movement models provide a wealth of transport statistics on a Eulerian grid and at different time intervals. These movement models differentiate between static and moving particles, which makes them useful for the visualization and analysis of the interaction between bar development and sediment transport. Movement models for the green

435 particles calculated on a 50 x 50 pixel grid are shown in Figure 11. Looking first at the $t = 50$ min frame, the moving particles are confined to a narrow corridor of active transport (e.g. only 1 grid square in j direction at the left side of the frame), below an area of mostly static particles. In the later frame (t =70 min), the previous transport corridor is mostly characterized by static particles, which document the development of the bar. Bar development is a complex process, however, and the transport corridor is relatively wide at $t = 90$ min (5 grid squares in j direction at left side of the frame), before narrowing again at $t =$

440 110 min. In the final frame there are fewer deposited particles visible on the left side of the frame (e.g. $j = 400$-450 px at $i =$ 600-650 px). The decrease in visible tracers is explained by the movement of fine sediment into this area that covers the deposited tracers rather than the transport of the tracers. Tracer movement is also noted in areas outside of the dominant corridor (e.g. $j = 350$-400 and $i = 800 – 850$ px at $t = 110$ min), but these are relatively small in number and are disconnected

https://doi.org/10.5194/egusphere-2025-4669
Preprint. Discussion started: 7 October 2025

from other grid squares with active movement, indicating that the particles re-deposit on the bar. The alternate bar on the right in the lower part of the frame appears at $t = 90$ min and is extended upstream by $t = 110$ min. As the experiment progressed, the active transport corridor occurs lower in the video frame on the left side of the frame, but the appearance of the downstream alternate bar results in bar growth towards the top of the frame between the latter two video segments. Movement vectors reflect this evolution as shown by all of the vectors pointing below horizontal at $t = 50$ min but many vectors are observed to be pointing above horizontal at $t = 110$ min. A final observation relates to the short duration paths. Based on a visual assessment, these paths are more numerous in areas with particles in motion, and particularly in areas that have both moving and static particles, which indicates that the post-processing algorithm is still having some difficulty connecting the track segments of moving paths.

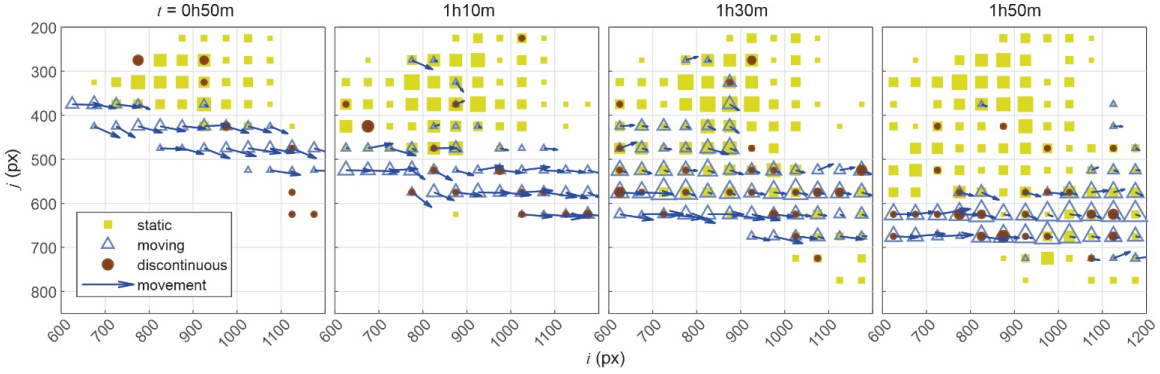

Figure 11 – Movement models of green particles at four moments in time. Note that the size of the symbols is scaled based on the number of particles in the respective static, moving and discontinuous classes, respectively, while the arrow indicates that direction and relative magnitude of the average vector of moving particles. The moving vectors are shown for a single time interval (1/60 s), but models for up to six time intervals (1/10 s) were created for the prediction of movement vectors.

4. Discussion

The goal of the current study, which was to develop a method to track the motion of particles in mixed fluvial bedload transport, was achieved using a combination of existing and novel algorithms for object tracking. The method allows a near-continuous measurement of particle transport paths of particles and assessments of the evolving size and spatial distributions of sediment particles on the channel bed, details that are critical for understanding sediment transport and bedform development (Lisle et al., 1991; Pyrce and Ashmore, 2003, 2005; Wilcock and Crowe, 2003; Ferrer-Boix and Hassan, 2014). The method uses a blob detection algorithm, which is different than the models that have been developed to date (Nokes, 2012; Heays et al., 2014; Terwisscha Van Scheltinga et al., 2021) and is thought to be more efficient for tracking large numbers of particles (Heyman, 2019). The key advances in the current paper were the novel application of the TracTrac algorithm, which includes a motion model that was sufficient in many cases to give preliminary estimates of track segments, and the development of a post-

https://doi.org/10.5194/egusphere-2025-4669
Preprint. Discussion started: 7 October 2025

processing algorithm to refine the tracklet predictions based on a grid-based probabilistic motion model that distinguished between static and moving particles and was able to account for missing detections up to 6 frames in duration. The advances were made possible by the application of a BOMC approach to distinguish sediment particles by size, which is similar to many other studies of sediment transport (Wilcock and Mcardell, 1993; Wilcock and Mcardell, 1997; Wong et al., 2007; Sklar et al., 2009; Ferrer-Boix and Hassan, 2014; Heays et al., 2014; Johnson et al., 2015; Chartrand et al., 2018; Reiterer et al., 2024), but the use of UV lights and fluorescent paint was tested for automatic particle tracking for the first time. This technique provided sufficient contrast in the videos so that particles could be tracked through the flowing water surface over bare and covered sediment beds. In this discussion we discuss the relevance of the work for descriptions of bar development, limitations of the method, the benefits of the post-processing method, future research directions, and recommendations for other researchers wishing to apply the methods.

The experiment was a replicate of an experiment by Peirce et al. (2021), where the sediment feed rate was held at 4 gs^{-1} and the alluvial bed cover developed over an initially bare bed. The current experiment allowed us to better understand bedform development in relation to sediment transport pathways. In particular, we were interested in documenting the 'parking lot' model of sediment transport proposed by Peirce et al. (2021), where the particles bump along a lateral bar and stop if they can find a suitable location or parking spot, and otherwise moving downstream. In the analysed videos, the analysis showed that it was the green particles (in the 87-97th percentiles of the supplied sediment) that formed the skeleton of the bar on the bare bed of the channel, while the smaller (61st-87th) and larger (97+) percentiles were underrepresented. Moving particles could deposit or be transported downstream depending on slight differences in the pathways of moving particles and their interactions with previously deposited particles. The edge of the bar next to the active transport corridor was not smooth, but rather characterized by small clusters of particles that could extend into the active corridor. A moving particle could become part of such a cluster if it was close enough to the bar edge, but particles that were slightly farther away tended to be routed around the clusters and trace a 'wavy' track. Some of the white tracks in Figure 10 show this pattern clearly. As the bar developed, finer particles tended to cover the skeleton of the bar made by coarser particles such that the coarse particles seemed to disappear even where there were no movement corridors that would show that they could have been removed from the bar (Figure 11). In the previous experiment, Peirce et al. (2021) were able to measure trends in exported sediment over time and visually noted some of the pathways that sediment took around bars, but the new ability to measure the tracks allows the simultaneous description of the bed state and sediment pathways. The clear benefit of the method is thus that the trends in surface distribution and transport can be quantified at any location with the flume.

This method was found to give good results under optimal conditions, but not all results were of sufficient quality to use for the intended analysis. The unattributed short segments of detections – the discontinuous motions – are instructive because they predominantly occur in areas with other particles in motion (Figures 8 and 11). Areas with static and moving particles in the same time interval seem to be particularly vulnerable to these unattributed detections. This makes intuitive sense given that it is more difficult to visually distinguish tracer particles that move quickly or appear to merge with other static particles as they pass over top. Particles that are interacting with others in a partially mobile area of the bed are also more likely to experience

https://doi.org/10.5194/egusphere-2025-4669
Preprint. Discussion started: 7 October 2025

abrupt accelerations and decelerations due to particle-to-particle impacts that make it difficult for motion models to correctly attribute positions to the right track segment. Water surface reflections and fast-moving particles can also result in time gaps. Despite these difficulties, the methods performed well in a range of particle densities and bed cover scenarios, and the discontinuous data is likely still valuable to help identify the active transport corridors.

The post-processing was necessary to get an adequate result, given that the TracTrac results left too many short segments and interrupted tracks to get reliable information about the numbers of tracks and their durations. The main physical difference found between our case of partial sediment transport and the cases tested by Heyman (2019), which included a granular avalanche and a flock of geese, is that all the Heyman tracked objects were in motion. There were no cases where objects within a given area of the image could be either at rest or in motion at the same time, which made it possible to infer likely displacements for a given object based on its proximity to other objects. In our case, moving objects could move right over static objects and it was necessary to: a) isolate the moving objects before calculating motion models; and b) pair static track segments to reduce the possibility of confusion with moving tracks. A key image difference is that all of the Heyman tracked objects were assumed to be visible in all video frames. In the current videos, the need to record through the water surface, which could have small waves, and the high speed of some of the moving particles meant that not all objects were detected in every frame. Our post-processing method improves on the TracTrac motion models by taking advantage of the relatively slow evolution of the spatial differences in sediment transport and averaging motions over all of the image segments in each time interval. As shown in Figure 11, for example, the active transport corridor moves slowly down through the field of view in our study, but it can also be assumed to be sufficiently constant over any time interval, such that it is possible to generate a probabilistic understanding of bed activity and deposition areas. The TracTrac motion model uses a position predictor step to account for the likely trajectory of each particle, but still follows with the Euclidean distance to identify the most likely paired position to complete a tracklet. By using a Mahalnobis distance, the new algorithm allows tracklets to be accepted or rejected based on a probabilistic understanding of displacement distances and angles. By creating a model for different time gaps, the new approach also allows for missed detections in some frames. The resulting grid-based motion models is also a useful result that could be used to compare with 2D grid-based hydro- and morphodynamic models.

The TracTrac model and post-processing steps are currently reliant on a number of parameter values that have not been adequately tested for different applications. For example, the thresholds to break low probability tracklets and classify tracklets in short/long and static/moving categories were hard-coded. Similarly, the values for the TracTrac parameters C_{NF}, C_{BS}, and C_{PN} were found iteratively and have not been optimized. However, despite the ad hoc approach we took to find appropriate values, some trends emerged in terms of the magnitude of these parameters relative to each other and particle sizes (Table 2). Further testing with more videos in different experiments is recommended to develop objective approaches to tuning these parameters. Future research should also explore the physical scenarios within which the algorithms will be sufficient to give adequate results.

For future applications of the algorithms, recommendations to maximize the quality of the results include:

https://doi.org/10.5194/egusphere-2025-4669
Preprint. Discussion started: 7 October 2025

1. *Assess the trade-off between camera frame field-of-view, sediment size, particle size resolution, and bedform scale.* It was found that the green particles, which had a mean diameter of 3.2 mm or 7.0 pixels were reliably detected. However, the smaller orange sizes, which had a mean diameter of 1.8 mm, often appeared larger but more blended with the blue/white background color so that it was challenging to extract much useful information from their analysis. Assuming that the green particles are the lower limit for accurate detection, the field of view for the current camera settings (1920 pixels) would be limited to the equivalent of 274 particle diameters or 0.88 m in real coordinates. This was the case here for the current study, which looked at alternate bars formed over a distance < 1.0 m in a channel approximately 0.20 m wide (Figure 1). The resolution was insufficient however, for accurately capturing the motion of the median size (D_{50} = 0.92 mm) which, assuming 7.0 px per particle diameter to for error-free detection, would require a reduction of the field of view to only ~ 0.25 m. This smaller field of view would have restricted the ability to resolve questions related to bar evolution with the current apparatus. Other options to enlarge the field of view while maintaining sufficient resolution of the particles could include higher resolution camera sensors or multiple cameras.
2. *Optimize the image brightness, frame rate, and shutter speed of the camera*. In our application, the orange particles moved rapidly over the bare bed in a preferred transport corridor just on the edge of the developing bar. Within this corridor, it was hard to reliably detect and connect detected positions of the particles. Rapidly moving particles tend to result in a relatively long shape due to the movement, which also results in dimmer colors and possible missed detections. Brighter lighting and faster shutter speeds are needed to ensure that the particles are clear and 'frozen'. The ROI should have a consistent brightness to ensure that the color segmentation thresholds are also consistent across the image frame. If it is possible to obtain high-quality images at sufficient frame rates then it may be possible to obtain a set of images in which the Cartesian distance between successive detections of a particle is less than the distance between objects, in which case motion recognition is relatively easy with standard particle tracking velocity algorithms (Heyman, 2019).
3. *Keep tracer classes within a narrow size range and limit the spatial concentration of each class.* A narrow size range will ensure that the blob-detection and filtering procedures work as intended. Particles that are too large or too small for the filtering algorithm are likely to be divided into multiple detected particles or filtered out, respectively. Limiting the spatial concentration of each class will reduce the risk of detection confusion related to amalgamated particles and tracers passing over each other.
4. *Test all colors under experimental conditions to ensure that they can be reliably differentiated.* For the current experiment, it was not obvious *a priori* how difficult it would be to separate the image by color, so only three colors were used. Nevertheless, there was some confusion due to the effect of the water and ambient lighting that was hard to eliminate in the lab (for example, a safety light on one end of the flume). More colors will allow for more sediment size classes to be tracked using this method, but this advantage must be balanced with the risk that color segmentation will introduce errors into the analysis.

https://doi.org/10.5194/egusphere-2025-4669
Preprint. Discussion started: 7 October 2025

5.0 Conclusions

A new particle tracking method was developed to allow characterization of the interaction between sediment particles in transport and sedimentary bedforms in flume experiments. The method is novel because it: a) achieves the necessary contrast for image analysis using ultraviolet lights and fluorescent paint; b) segments the images to obtain colour-specific videos of select sediment size classes in the mixed bed; c) applies a blob-detection method included in the standalone TracTrac software to detect and track particles at rest and in motion; and d) includes a custom post-processing algorithm that uses a grid-based probabilistic motion model to reduce errors that are inherent in the noisy process of sediment transport. The method was developed as an open-source software written in Matlab and available as three separate algorithms to segment a video file by colour, create a dataset for validation, and run the post-processing algorithm. To document the methods, we applied the algorithms to a set of videos taken during a laboratory experiment in which a pair of alternate bars and a cross-over central bar were forming in a shallow flume with non-cohesive sand and gravel transport. When the method works well, as it did in the current videos for particles in the 2.4-4.0 mm size class (~7 pixels in nominal diameter), it was able to achieve a minimum error of +7% in the number of tracks and -20% in the average duration of tracks. This type of accuracy allowed a detailed consideration of the sediment pathways and locations of static particles to show how the active sediment corridor shifted across the frame as a lateral bar developed and deflected from the initial trajectories as an alternate lateral bar formed. Success of the method however, is reliant on accurate detection of tracer positions and the ability to predict connections between two identified positions with a motion model. The post-processing motion model we developed was shown to massively improve on the connections between particle locations, with order of magnitude reductions of errors in both the total number and duration of automatically determined tracks. The methods are imperfect however, and users should consider the provided recommendations related to particle resolution, image quality, tracer seeding design, and color segmentation. It is also recommended that further testing be undertaken to assess whether values for subjective parameters could be arrived at using a more objective approach where parameters are functions of the resolution of tracer particles in the images.

Code availability

All codes are available to download at github\macvicab\ParticleTracker.

Data availability

Manually annotated particle tracks and the results of all analysis steps for the video taken at 90 min since the start of the experiment are available at github\macvicab\ParticleTracker\sample.

https://doi.org/10.5194/egusphere-2025-4669
Preprint. Discussion started: 7 October 2025

Video supplement

The video taken at 90 min since the start of the experiment is available as a video supplement (P1000022_res.mp4), as are the segmented videos for the 1.18-2.36 mm, 2.36-4 mm, and 4-5.6 mm size classes painted pink, green and orange, respectively (respective videos saved as P1000022ORANGE.mp4, P1000022GREEN.mp4, and P1000022PINK.mp4). All videos are 1920 x 1080 px, 10 s in duration, and recorded at 60 fps.

Author contribution

Author's individual contributions to the work are detailed using the CRediT taxonomy as follows: conceptualization by FAM and BJM; data curation by LM and BJM; formal analysis by MI, FAM, and BJM; funding acquisition by BJM; investigation by MI, LM, and FAM; methodology by all; project by BJM, software by MI, FAM, and BJM; supervision by BJM, validation by LM and BJM; visualization by MI, FAM, and BJM; original draft preparation by MI, FAM, and BJM; editing by all.

Competing interests

The authors declare that they have no conflict of interest.

Acknowledgements

The authors are grateful to many fruitful discussions with Dr. Peter Ashmore during this long process of developing a useful algorithm. Mark Hummel was invaluable in the construction and maintenance of the flume, as were members of the Engineering Machine Shop that contributed to the modifications of the Sandee flume that made this research possible.

Financial Support

This work was funded by two National Sciences and Engineering Research Council of Canada (NSERC) grants including a Strategic Partnership Grant (463321) and a Discovery Grant (2023-03720) awarded to BM.

References

AECOM (2011). Wilket Creek Rehabilitation Project Master Plan – Hydraulic Analysis. Retrieved from: http://www.trca.on.ca/dotAsset/201894.pdf .

Reprint of: Mahalanobis, P.C. (1936) "On the Generalised Distance in Statistics.", Sankhya A, 80, 1-7, 10.1007/s13171-019-00164-5, 2018.

Ancey, C.: Bedload transport: a walk between randomness and determinism. Part 1. The state of the art, Journal of Hydraulic Research, 58, 1-17, 10.1080/00221686.2019.1702594, 2020a.

Ancey, C.: Bedload transport: a walk between randomness and determinism. Part 2. Challenges and prospects, Journal of Hydraulic Research, 58, 18-33, 10.1080/00221686.2019.1702595, 2020b.

https://doi.org/10.5194/egusphere-2025-4669
Preprint. Discussion started: 7 October 2025

Bankert, A. R. and Nelson, P. A.: Alternate bar dynamics in response to increases and decreases of sediment supply, Sedimentology, 65, 702-720, 10.1111/sed.12399, 2018.
Battisacco, E., Franca, M. J., and Schleiss, A. J.: Sediment replenishment: Influence of the geometrical configuration on the morphological evolution of channel-bed, Water Resources Research, 52, 8879-8894, 10.1002/2016WR019157, 2016.
Bevan, V., MacVicar, B. J., Chapuis, M., Ghunowa, K., Papangelakis, E., Parish, J., and Snodgrass, W.: Enlargement and evolution of a semi-alluvial creek in response to urbanization, Earth Surface Processes and Landforms, 43, 2295-2312, 10.1080/00221686.2018.1522379, 2018.
Campagnol, J., Radice, A., Ballio, F., and Nikora, V.: Particle motion and diffusion at weak bed load: Accounting for unsteadiness effects of entrainment and disentrainment, Journal of Hydraulic Research, 53, 633-648, 10.1080/00221686.2015.1085920, 2015.
Chartrand, S. M., Jellinek, A. M., Hassan, M. A., and Ferrer-Boix, C.: Morphodynamics of a Width-Variable Gravel Bed Stream: New Insights on Pool-Riffle Formation From Physical Experiments, Journal of Geophysical Research: Earth Surface, 123, 2735-2766, 10.1029/2017JF004533, 2018.
Drake, T. G., Shreve, R. L., Dietrich, W. E., P.J.Whiting, and Leopold, L.: Bedload transport of fine gravel observed by motion picture photography, Journal of Fluid Mechanics, 192, 193-217, 1988.
Elgueta-Astaburuaga, M. A. and Hassan, M. A.: Experiment on temporal variation of bed load transport in response to changes in sediment supply in streams, Water Resources Research, 53, 763-778, 10.1002/2016WR019460, 2017.
Elgueta-Astaburuaga, M. A., Hassan, M. A., Saletti, M., and Clarke, G. K. C.: The Effect of Episodic Sediment Supply on Bedload Variability and Sediment Mobility, Water Resources Research, 54, 6319-6335, 10.1029/2017WR022280, 2018.
Ermilov, A. A., Fleit, G., Conevski, S., Guerrero, M., Baranya, S., and Rüther, N.: Bedload transport analysis using image processing techniques, Acta Geophys., 70, 2341-2360, 10.1007/s11600-022-00791-x, 2022.
Fan, N., Xie, Y., and Nie, R.: Bed load transport for a mixture of particle sizes: Downstream sorting rather than anomalous diffusion, Journal of Hydrology, 553, 26-34, 10.1016/j.jhydrol.2017.07.012, 2017.
Fathel, S. L., Furbish, D. J., and Schmeeckle, M. W.: Experimental evidence of statistical ensemble behavior in bed load sediment transport, Journal of Geophysical Research F: Earth Surface, 120, 2298-2317, 10.1002/2015JF003552, 2015.
Ferrer-Boix, C. and Hassan, M. A.: Influence of the sediment supply texture on morphological adjustments in gravel-bed rivers, Water Resources Research, 50, 8868-8890, 10.1002/2013WR015117, 2014.
Frostick, L., McLelland, S. J., and Mercer, T. G.: Users Guide to Physical Modelling and Experimentation: Experience of the HYDRALAB Network, IAHR Design Manual, CRC Press, London, Uk2011.
Hassan, M. A. and Roy, A. G.: Coarse particle tracing in fluvial geomorphology, in: Tools in Fluvial Geomorphology, John Wiley & Sons, Ltd, 306-323, 10.1002/9781118648551.ch14, 2016.
Heays, K. G., Friedrich, H., Melville, B. W., and Nokes, R.: Quantifying the dynamic evolution of graded gravel beds using particle tracking velocimetry, Journal of Hydraulic Engineering, 140, 10.1061/(ASCE)HY.1943-7900.0000850, 2014.
Heyman, J.: TracTrac: A fast multi-object tracking algorithm for motion estimation, Comput. Geosci., 128, 11-18, 10.1016/j.cageo.2019.03.007, 2019.
Hodge, R., Hoey, T., Maniatis, G., and Leprêtre, E.: Formation and erosion of sediment cover in an experimental bedrock-alluvial channel, Earth Surface Processes and Landforms, 41, 1409-1420, 10.1002/esp.3924, 2016.
Humphries, R., Venditti, J. G., Sklar, L. S., and Wooster, J. K.: Experimental evidence for the effect of hydrographs on sediment pulse dynamics in gravel-bedded rivers, Water Resources Research, 48, 10.1029/2011WR010419, 2012.
Iseya, F. and Ikeda, H.: Pulsations in bedload transport rates induced by a longitudinal sediment sorting: a flume study using sand and gravel mixtures, Geographiska Annaler, 69A, 15-27, 1987.
Johnson, J. P. L., Aronovitz, A. C., and Kim, W.: Coarser and rougher: Effects of fine gravel pulses on experimental step-pool channel morphodynamics, Geophysical Research Letters, 42, 8432-8440, 10.1002/2015GL066097, 2015.
Lajeunesse, E., Malverti, L., and Charru, F.: Bed load transport in turbulent flow at the grain scale: Experiments and modeling, J. Geophys. Res., 115, F04001, 10.1029/2009jf001628, 2010.
Liébault, F., Piégay, H., Cassel, M., and Arnaud, F.: Bedload tracing with RFID tags in gravel-bed rivers: Review and meta-analysis after 20 years of field and laboratory experiments, Earth Surface Processes and Landforms, 49, 147-169, https://doi.org/10.1002/esp.5704, 2024.
Lisle, T. E., Ikeda, H., and Iseya, F.: Formation of stationary alternate bars in a steep channel with mixed-size sediment: A flume experiment, Earth Surface Processes and Landforms, 16, 463-469, 1991.
MacKenzie, L. G. and Eaton, B. C.: Large grains matter: contrasting bed stability and morphodynamics during two nearly identical experiments, Earth Surface Processes and Landforms, 42, 1287-1295, 10.1002/esp.4122, 2017.
McKie, C. W., Juez, C., Plumb, B. D., Annable, W. K., and Franca, M. J.: How Large Immobile Sediments in Gravel Bed Rivers Impact Sediment Transport and Bed Morphology, Journal of Hydraulic Engineering, 147, 10.1061/(ASCE)HY.1943-7900.0001842, 2021.
Nelson, P. A., Bolla Pittaluga, M., and Seminara, G.: Finite amplitude bars in mixed bedrock-alluvial channels, Journal of Geophysical Research: Earth Surface, 119, 566-587, 10.1002/2013JF002957, 2014.
Nelson, P. A., Dietrich, W. E., and Venditti, J. G.: Bed topography and the development of forced bed surface patches, J. Geophys. Res., 115, F04024, 10.1029/2010jf001747, 2010.

https://doi.org/10.5194/egusphere-2025-4669
Preprint. Discussion started: 7 October 2025

Nokes, R.: Streams v. 2.00. System theory and design, University of Canterbury, Christchurch, New Zealand, 2012.
Paiement-Paradis, G., Marquis, G., and Roy, A.: Effects of turbulence on the transport of individual particles as bedload in a gravel-bed river, Earth Surface Processes and Landforms, 36, 107-116, 10.1002/esp.2027, 2011.
Papangelakis, E. and MacVicar, B.: Process-based assessment of success and failure in a constructed riffle-pool river restoration project, River Research and Applications, 36, 1222-1241, 10.1002/rra.3636, 2020.
Peirce, S., MacVicar, B. J., Papangelakis, E., Vervynck, L., and Ashmore, P.: Experiments on restoring alluvial cover using gravel augmentation in a variable width channel with irregular meanders, Geomorphology, 379, 107585, https://doi.org/10.1016/j.geomorph.2020.107585, 2021.
Pyrce, R. S. and Ashmore, P. E.: Particle path length distributions in meandering gravel-bed streams: Results from physical models, Earth Surface Processes and Landforms, 28, 951-966, 2003.
Pyrce, R. S. and Ashmore, P. E.: Bedload path length and point bar development in gravel-bed river models, Sedimentology, 52, 839-857, 810.1111/j.1365-3091.2005.00714.x, 2005.
Radice, A., Sarkar, S., and Ballio, F.: Image-based Lagrangian particle tracking in bed-load experiments, Journal of Visualized Experiments, 2017, 10.3791/55874, 2017.
Rebai, D., Radice, A., and Ballio, F.: Traveling or Jiggling: Particle Motion Modes and Their Relative Contribution to Bed-Load Variables, Journal of Geophysical Research: Earth Surface, 129, 10.1029/2024JF007637, 2024.
Reiterer, K., Gold, T., Hauer, C., Habersack, H., and Sindelar, C.: A Novel Laboratory Technique for Measuring Grain-Size-Specific Transport Characteristics of Bed Load Pulses, Water Resources Research, 60, 10.1029/2023WR036712, 2024.
Roseberry, J. C., Schmeeckle, M. W., and Furbish, D. J.: A probabilistic description of the bed load sediment flux: 2. Particle activity and motions, Journal of Geophysical Research: Earth Surface, 117, F03032, 10.1029/2012JF002353, 2012.
Sklar, L. S., Fadde, J., Venditti, J. G., Nelson, P., Wydzga, M. A., Cui, Y. T., and Dietrich, W. E.: Translation and dispersion of sediment pulses in flume experiments simulating gravel augmentation below dams, Water Resources Research, 45, 10.1029/2008wr007346, 2009.
Terwisscha van Scheltinga, R. C., Coco, G., and Friedrich, H.: Sediment Particle Velocity and Activity During Dune Migration, Water Resources Research, 57, 10.1029/2020WR029017, 2021.
Wilcock, P. R.: Toward a practical method for estimating sediment-transport rates in gravel-bed rivers, Earth Surface Processes and Landforms, 26, 1395-1408, 2001.
Wilcock, P. R. and Crowe, J. C.: Surface-based transport model for mixed-size sediment, Journal of Hydraulic Engineering, 129, 120-128, 10.1061/(ASCE)0733-9429(2003)129:2(120), 2003.
Wilcock, P. R. and Kenworthy, S. K.: A two-fraction model for the transport of sand/gravel mixtures, Water Resources Research, 38, 2002.
Wilcock, P. R. and McArdell, B. W.: Surface-based fractional transport rates: mobilization thresholds and partial transport of a sand-gravel sediment, Water Resources Research, 29, 1297-1312, 1993.
Wilcock, P. R. and McArdell, B. W.: Partial transport of a sand/gravel mixture, Water Resources Research, 33, 235-245, 1997.
Wong, M., Parker, G., DeVries, P., Brown, T. M., and Burges, S. J.: Experiments on dispersion of tracer stones under lower-regime plane-bed equilibrium bed load transport, Water Resources Research, 43, 2007.
Zimmermann, A. E., Church, M., and Hassan, M. A.: Video-based gravel transport measurements with a flume mounted light table, Earth Surface Processes and Landforms, 33, 2285-2296, 10.1002/esp.1675, 2008.